Laboratory of Computational Physics

by Luca Cassia

Dipartimento di Fisica, Università di Milano-Bicocca
I-20126 Milano, Italy

Email: l.cassia@campus.unimib.it

Table of contents

1 Potts Model 2*d*

The 2-dimensional Potts Model constitutes a generalization of the Ising Model to a generic number $q \in \mathbb{N}$ of states for the spin variable. A useful way to picture the space of states of a Potts spin variable is to map it to the space $U(1) \subset \mathbb{C}$ of unimodular complex numbers. We represent each state p with the p^{th} complex q-root of the unity in $\mathbb{C}$:

$$p \mapsto e^{\frac{2\pi i}{q} p} \in U(1) \tag{1}$$

Lets consider a 3-state Potts system of $L \times L$ spins situated on the points of a regular square lattice with periodic boundary conditions (PBC) in both directions, as for the Ising Model. Each spin interacts with its nearest neighbours inside the lattice, with an Hamiltonian:

$$H = -\sum_{\langle i,j \rangle} \delta_{\sigma_i,\sigma_j} \tag{2}$$

where the sum is taken only over the set of unordered pairs $\langle i, j \rangle$ such that σ_i and σ_j are nearest neighbours. The implementation of the MH algorithm is completely analogous to that for the ising model, while for the SW algorithm we need to modify the probability with which to activate the link between neighbouring spins. In fact, the partition function can be written as:

$$Z[\beta] = \sum_{\{\sigma\}} \mathrm{e}^{\beta \sum_{\langle ij \rangle} \delta_{\sigma_i \sigma_j}} = \sum_{\{\sigma\}} \prod_{\langle ij \rangle} \mathrm{e}^{\beta \delta_{\sigma_i \sigma_j}} \tag{3}$$

using the Fortuin-Kasteleyn representation we can write:

$$\mathrm{e}^{\beta \delta_{\sigma_i \sigma_j}} = 1 + (\mathrm{e}^{\beta} - 1)\delta_{\sigma_i \sigma_j} = \mathrm{e}^{\beta} \left[\mathrm{e}^{-\beta} + (1 - \mathrm{e}^{-\beta})\, \delta_{\sigma_i \sigma_j}\right] \tag{4}$$

therefore we can immediately read the probability of establishing a link between neighbouring spins as:

$$p = 1 - \mathrm{e}^{-\beta} \tag{5}$$

1.1 Thermalization

As for the case of the Ising Model, we opted for a cold start approach. In (Fig.1) we present the thermalization process for MH and SW at various temperatures and for two different volumes: 32^2 and 64^2.

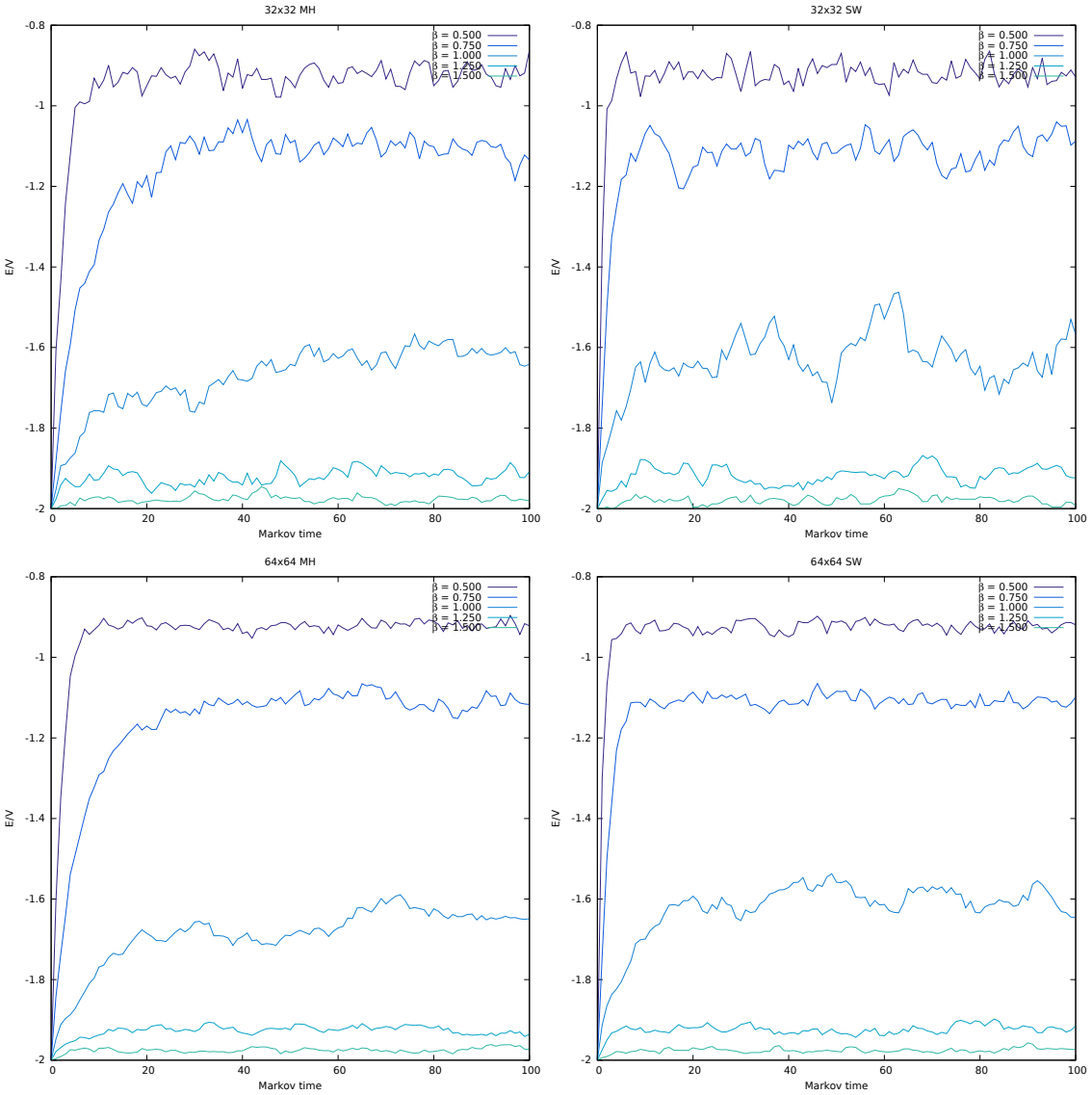

Figure 1. Thermalization process of the energy density on a lattice 32×32 in the top two pictures and 64×64 in the bottom two. MH on the left, SW on the right.

As expected, the MH algorithm has a slower mixing rate due to the critical slowing down effect near the critical inverse temperature:

$$\beta_c = \log\left(1+\sqrt{3}\right) \approx 1.00505254... \tag{6}$$

For this reason we focus only on the study of the model through the implementation of the much more efficient SW algorithm. The thermalization time is taken to be 1000 Markov steps.

1.2 Autocorrelation Times

We now study the correlations present between consecutive configurations sampled by the two algorithms in order to obtain the characteristic time after which we can consider two configurations to be statistically independent. This is called *integrated autocorrelation time* and is computed in the following way:

$$\tau_{\mathcal{O},\text{int}} = \frac{1}{2} + \sum_{k=1}^{k_{\max}} R(k) \tag{7}$$

where $\mathcal{O}$ is the physical observable for which we compute autocorrelation and $R(k)$ is defined as:

$$R(k) = \frac{1}{(n-k)\,\sigma^2} \sum_{t=1}^{n-k} (\mathcal{O}_t - \mu)\,(\mathcal{O}_{t+k} - \mu) \tag{8}$$

here n is the total number of samples of $\mathcal{O}$ and μ, σ^2 are the mean and variance of the process. For large time separations k, $R(k)$ decays exponentially:

$$R(k) \xrightarrow{k\to\infty} r\mathrm{e}^{-k/\tau_{\mathcal{O},\exp}} \tag{9}$$

which defines the exponential autocorrelation time $\tau_{\mathcal{O},\exp}$.

We immediately see from (Fig.2) that the MC process is strongly correlated in time particularly near the phase transition:

Figure 2. Comparison of the energy for the two algorithms at $\beta = \beta_c$ and $L = 32$. (Left) MH (Right) SW.

We now compute the autocorrelation time τ_{int} for the observable $e = E/V$ using formula (7):

Figure 3. Plot of the integrated autocorrelation time near the phase transition for the MH algorithm. The raw data was obtained from a simulation of 10^6 measurements on a lattice 32×32. The fit in the center is not very accurate because near β_c the autocorrelation time becomes very large and the interval $[0, 2000]$ becomes too small for a reliable estimate of τ_{int}.

Figure 4. Plot of the integrated autocorrelation time near the phase transition for the SW algorithm. The raw data was obtained from a simulation of 10^5 measurements on a lattice 32×32.

The data is fitted using the function:

$$\tau_{\mathrm{int}}(k_{\max}) = \tau_{\mathrm{int}}\left[1 - \frac{2\,\tau_{\exp}}{2\,\tau_{\exp}+1}\,\mathrm{e}^{-k_{\max}/\tau_{\exp}}\right] \tag{10}$$

which is the exact solution for a bivariate gaussian process.

As we can see, near the phase transition the autocorrelation time for the MH process becomes very large compared to the autocorrelation time of the SW process (Fig.5). In fact due to the critical slowing down of the MH algorithm, we have $\tau_{\mathrm{int}}^{\mathrm{MH}} \sim 100$ compared to an autocorrelation time $\tau_{\mathrm{int}}^{\mathrm{SW}} \sim 5$ for SW.

Figure 5. Plot of the integrated autocorrelation time as a function of $x = \frac{\beta - \beta_c}{\beta_c}$ for $L = 32$.

We remark that the peak is slightly off centered because of the finite size of the lattice (pseudocritical point $\beta_c(V) < \beta_c(\infty)$).

1.3 Observables

The main observables of interest for this system are the energy density e and the magnetization m:

$$e = E/V, \qquad E = \langle \mathcal{H} \rangle, \qquad V = L^d \tag{11}$$

$$m = M/V, \qquad M = \langle \mathcal{M} \rangle, \qquad \mathcal{M} = \left| \sum_i \sigma_i \right| \tag{12}$$

Thanks to the analytical solution of the $2d$ Ising model, first obtained by Onsager, we are able to compare the estimators computed by numerical simulations with their exact values obtained analytically.

The samples and the errors are collected employing the binning procedure of the previous section. For each inverse temperature we compute the estimate of the generic observable $\mathcal{O}$ from 10^5 measurements for MH and 10^4 for SW.

Figure 6. Energy density as a function of β. MH on the left and SW on the right.

Figure 7. Magnetization as a function of β. MH on the left and SW on the right.

We find that the simulation data are remarkably close to the exact solution both for the energy density and for the magnetization expecially for large sizes of the lattice. The only departure from Onsager's solution is in the paramagnetic phase of the magnetization plot: there we observe that the exact solution goes abruptly to zero before the critical point, while the numerical data seems to interpolate a smooth function. This is imputable to the finite size of the lattice used for the simulation. It is indeed a well known fact that discontinuities and divergences only appear in the thermodinamic limit of infinite size, which is precisely the premise of Onsager's solution. In fact, the numerical solution approaches more and more the exact one as the size of the lattice increases.

We also plot the heat capacity:

$$C = \frac{\beta^2}{V} \langle (\mathcal{H} - \langle \mathcal{H} \rangle)^2 \rangle \tag{13}$$

Figure 8. Heat capacity as a function of β. MH on the left and SW on the right.

and the magnetic susceptibility:

$$\chi = \frac{\beta}{V} \langle (\mathcal{M} - \langle \mathcal{M} \rangle)^2 \rangle \tag{14}$$

Figure 9. Magnetic susceptibility as a function of β. MH on the left and SW on the right.

As we immediately see from (Fig.8) and (Fig.9) the peak of the curve is progressively shifted to the infinite-size limit value β_c as we approach larger and larger sizes of the lattice:

$$\lim_{L \to \infty} \beta_{\max}(L) = \beta_c = \ln\left(1 + \sqrt{2}\right)/2 \tag{15}$$

1.4 β Critical

From a power law fit of the points near the peak of each dataset we obtain estimates for the pseudocritical β-values at finite sizes $L = 8, 16, 32, 64$.

Figure 10. Fit of the heat capacity and susceptibility peaks (MH).

L	$\beta_{\max}(C)$	$\beta_{\max}(\chi)$
8	0.42400 ± 0.00043	0.39448 ± 0.00051
16	0.43086 ± 0.00086	0.41541 ± 0.00055
32	0.43613 ± 0.00103	0.42620 ± 0.00141
64	0.43718 ± 0.00065	0.43405 ± 0.00075

Table 1. Pseudocritical β-values obtained by polynomial fit of the peaks of C and χ (MH).

The polynomial function we used for the fit is:

$$f(\beta) = A + B\,(\beta - \beta_{\max})^2 + C\,(\beta - \beta_{\max})^3 \tag{16}$$

where we omitted the term of order one since it should be zero near the maximum of the function.

Figure 11. Fit of the heat capacity and susceptibility peaks (SW).

L	$\beta_{\max}(C)$	$\beta_{\max}(\chi)$
8	0.42296 ± 0.00073	0.39295 ± 0.00059
16	0.43174 ± 0.00090	0.41729 ± 0.00061
32	0.43524 ± 0.00078	0.42686 ± 0.00078
64	0.43788 ± 0.00040	0.43481 ± 0.00042

Table 2. Pseudocritical β-values obtained by polynomial fit of the peaks of C and χ (SW).

Remark: the estimates of the heat capacity and magnetic susceptibility of the MH algorithm are very accurate for small values of L where we employed a large dataset of 10^5 measurements and the autocorrelation time is relatively small. For large values of L the autocorrelation time grows very large compared to the size of the dataset and the estimates become less accurate.

The situation for the SW algorithm is different since the autocorrelation time in this case is always under control. However the smaller size of the dataset results in less accurate estimates expecially at small lattice sizes where the MH algorithm is most efficient.

We can now obtain an estimate of β_c from a power law fit to the location of the maxima $\beta_{\max}$:

$$\beta_{\max} = \beta_c - c\,L^{-\nu} \tag{17}$$

Figure 12. Pseudocritical inverse temperature fit. MH on the left, SW on the right. The purple lines are relative to the heat capacity C while the green ones to the magnetic susceptibility χ.

The result of the fit are:

	$\beta_c(C)$	$\beta_c(\chi)$
MH	0.43986 ± 0.00234	0.44287 ± 0.00173
SW	0.44007 ± 0.00105	0.44071 ± 0.00322

These results are very close to the exact solution but still they could be greatly improved by taking more points expecially at larger values of L for which C and χ are more peaked.

1.5 Probability Distribution Functions

We study the probability distribution of the magnetization for a lattice of size $L = 8$. The energy and magnetization levels of a discrete system are quantized. In particular, for a Potts Model on a square lattice of size L^2 with PBC, there are exactly $\frac{1}{2}(L^2+1)(L^2+2)$ magnetization levels distributed as in (Fig.13):

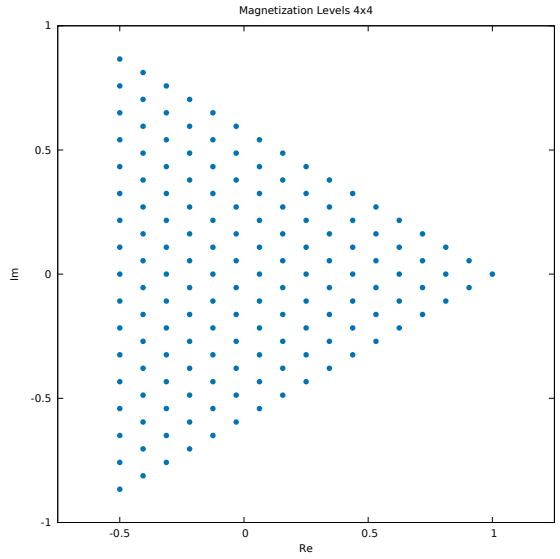

Figure 13. Magnetization levels of the Potts Model on a 4×4 lattice.

With this consideration one can construct the probability distribution function of the magnetization just by counting the number of samples in each level (for L not too large). In (Fig.14) and (Fig.15) we show the PDFs of m for both of the algorithms and for various values of β:

Figure 14. Probability distribution functions of m obtained from 10^6 sweeps of MH on a lattice 8×8.

By looking at the PDFs of m we can witness the formation of a 2-fold degeneracy of the ground state of the system for $\beta > \beta_c$. Moreover, if we get close to the phase transition, we see that the distribution $P(m, \beta)$ becomes almost flat at $m = 0$ before "splitting" into the sum of two PDFs for the two degenerate vacua. This implies that near β_c the distribution does not have a well defined second cumulant, which is precisely the magnetic susceptibility.

Figure 15. Probability distribution functions of m obtained from 10^6 sweeps of SW on a lattice 8×8.

Since we used a cold start initialization, all our simulations at temperatures lower than T_c spontaneously broke the $\mathbb{Z}_2$ symmetry of the ground state to some value $m_0 > 0$. Having used a hot start initialization instead, we would have ended up with $m_0 = \pm|m_0|$ with probability $\frac{1}{2}$ each.

1.6 Spatial Correlations

The two-point correlation function is defined as:

$$G(\vec{r}_i - \vec{r}_j) = \langle \sigma_i \sigma_j \rangle \quad \sim \quad \exp(-|\vec{r}_i - \vec{r}_j| / \xi) \quad \text{for large} \quad |\vec{r}_i - \vec{r}_j| \tag{18}$$

where ξ is the correlation length of the system:

$$\xi = -\lim_{|\vec{r}| \to \infty} (|\vec{r}| / \ln G(\vec{r})) \tag{19}$$

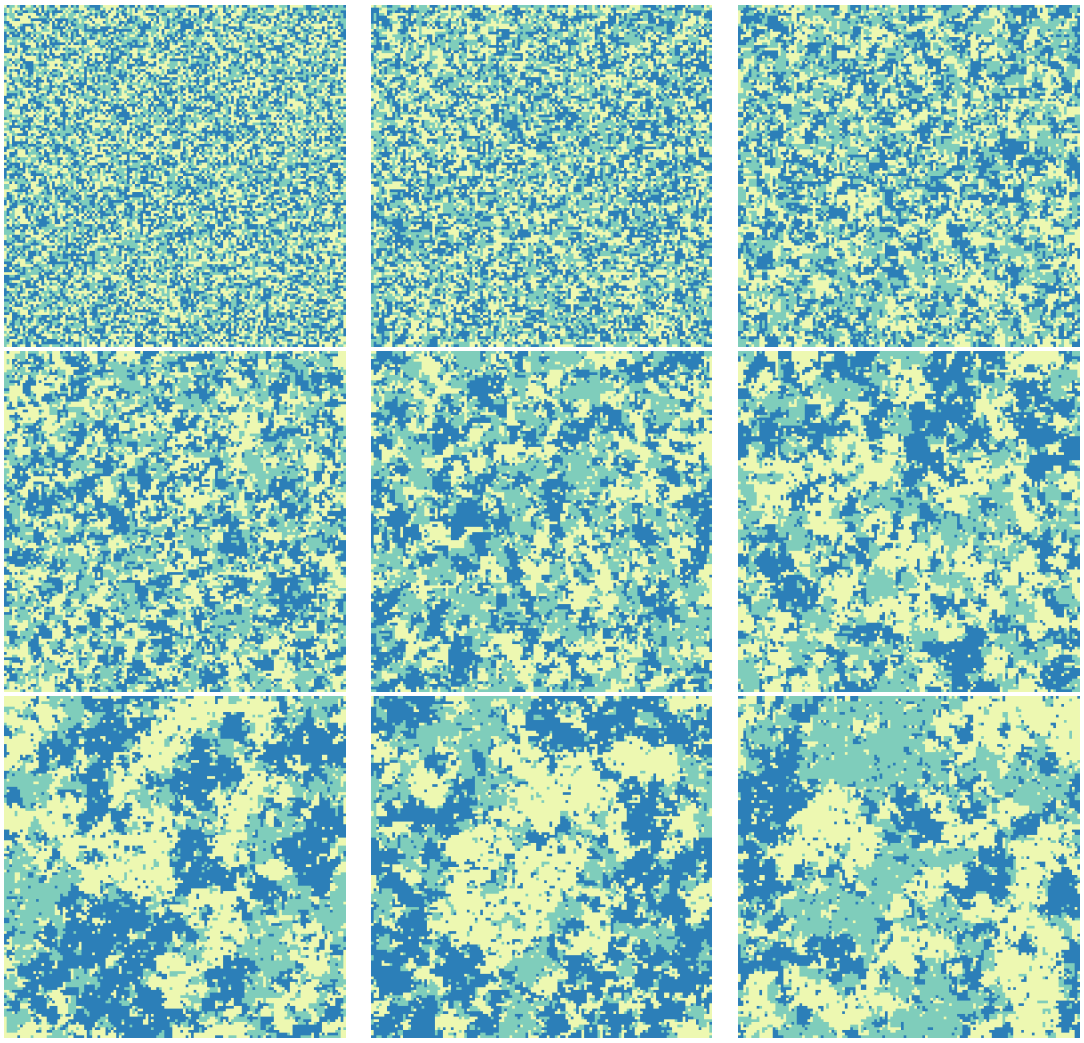

Figure 16. Ilustration of the growth of spatial correlations when criticality is approached on a lattice 128×128 : $\beta = 0.2, 0.5, 0.7, 0.8, 0.9, 0.95, 0.97, 0.98, 0.99$.

Since our system is finite and lives on a lattice, the rotational symmetry SO(2) of $\mathbb{R}^2$ is broken down to the discrete subgroup $\mathbb{Z}_4$ of $\frac{\pi}{2}$ rotations. We take advantage of this and the translational symmetry of the system to compute an improved version of the correlation function $G(\vec{r})$ by defining the observables:

$$S_x \equiv \frac{1}{L} \sum_{y=1}^{L} \sigma(x, y) \tag{20}$$

$$S_y \equiv \frac{1}{L} \sum_{x=1}^{L} \sigma(x, y) \tag{21}$$

where x and y are the two orthogonal directions in the lattice.

We can compute the correlation function as:

$$G(r) = \frac{1}{2} \left(\frac{1}{L} \sum_{x=1}^{L} S_x \, S_{x+r} + \frac{1}{L} \sum_{y=1}^{L} S_y \, S_{y+r} \right) \tag{22}$$

Because of the periodic boundary conditions on the lattice we also have that:

$$\sigma(x + a\,L, y + b\,L) = \sigma(x, y) \qquad \forall\,(a, b) \in \mathbb{Z}^2 \tag{23}$$

and therefore, the exponential form of G is modified to that of a hyperbolic cosine:

$$G(r) \sim \frac{1}{2}\left(\mathrm{e}^{\frac{r}{\xi}} + \mathrm{e}^{\frac{L-r}{\xi}}\right) \sim \cosh\left(\frac{r-\frac{L}{2}}{\xi}\right) \tag{24}$$

In (Fig.17) we can see the exponential decay of the correlation function at large distances.

Figure 17. Correlation functions for various values of β. The lattice size used is 128×128 in order to reduce finite-size effects. As a precaution, we considers an interval in β-space such that the correlation length is much smaller that the size of the lattice (approximately one order of magnitude smaller).

The correlation length diverges at the critical point as:

$$\xi \sim A\,|x|^{-\nu} \tag{25}$$

where ν is an example of critical exponent of the model. We plot the data obained from the previous fit using logarithmic scales on both axis. This way we can easily obtain the critical exponent ν from a linear fit:

$$\log(\xi) = \log(A) - \nu \log(|x|) \tag{26}$$

Figure 18. Plot of the correlation length dependence on the parameter $x = \frac{\beta - \beta_c}{\beta_c}$ for a lattice of size 128×128. MH on the left and SW on the right. The errors are computed by jackknife binning of the fit data from (Fig.17) through (24).

The results are:

$$\nu_{\mathrm{MH}} = 1.017 \pm 0.029 \tag{27}$$

$$\nu_{\mathrm{SW}} = 1.045 \pm 0.014 \tag{28}$$

Both results are compatible with the known exact value $\nu = 1$.

1.7 Finite Size Scaling

The main results of the finite size scaling (FSS) study are usually estimates of the critical temperature and the critical exponents characterizing the universality class of the transition. In the infinite-volume limit most of the expectation values one can compute from e and m exhibit singularities at the transition point. In finite systems, though, the singularities are smeared out and the standard observables scale according to:

$$m = L^{-\beta/\nu} f_m(y) + \ldots \tag{29}$$

$$C = C_{\mathrm{reg}} + L^{\alpha/\nu} f_C(y) + \ldots \tag{30}$$

$$\chi = L^{\gamma/\nu} f_\chi(y) + \ldots \tag{31}$$

where α, β, γ and ν are the critical exponents, $f_i(x)$ are FSS functions and y is the scaling variable. Near the phase transition the correlation length $\xi \sim x^{-\nu}$ is the only length scale with which to describe the physics of the system, therefore the only adimensional quantity we can contruct from it is:

$$y = L/\xi \sim L\,x^{\nu} = \left(L^{1/\nu} x\right)^{\nu} = L\,x \tag{32}$$

We now can remove any dependence on the scale of the system by rescaling the observables by the appropriate power of L given by the relative critical exponent. This way we expect each observable, expressed as functions of the scaling variable y, to collapses on the same curve $f_i(y)$ regardless of the value of L (at least in the vicinity of β_c).

ν	1
α	0
β	1/8
γ	7/4

Table 3. Exact critical exponents for the Ising model in 2d.

With a precedure completely analogous to that of (Sect.1.4), one could also obtain estimates for the crtical exponents α, β, γ and ν by extrapolating the infinite size limit.

Remark: we observe that since the exact value of exponent α of the model is zero, the quantity C should, in principle, not scale with the lattice size. In reality C has a logarithmic divergence at the critical point, hence we adopt the scaling law:

$$C \sim \log\left(L^{1/\nu}\right) \tag{33}$$

Figure 19. Finite Size Scaling study for the lattice sizes $8^2, 16^2, 32^2, 64^2$. Left MH, right SW. The top plot represents the scaling of the magnetization, the center one the magnetic susceptibility and the bottom one the heat capacity.